Absence of Space-Charge-Limited Current in Unconventional Field Emission

Cherq Chua, Chun Yun Kee, Yee Sin Ang[*] and L.K. Ang[†]

Science, Mathematics and Technology (SMT), Singapore University of Technology and Design, 8 Somapah Road, 487372, Singapore

(Received 21 May 2021; revised 27 October 2021; accepted 8 November 2021; published 9 December 2021)

For field emission (FE), it is widely expected that its emitting current density J will become space-charge-limited current (SCLC) within a gap spacing D biased at sufficiently large voltage V. In this paper, we reveal a peculiar finding in which this expected two-stage transition (from FE to SCLC) is no longer valid for FE not obeying the traditional Fowler-Nordheim (FN) law. By employing a generalized FN scaling of $\ln(J/E_s^k) \propto -1/E_s$, where E_s is the surface electric field at the cathode, we show the existence of a *critical exponent* $k_c \equiv 3/2$ where unusual behaviors occur for $k < k_c$: (a) only FE at small D (no transition to SCLC possible) and (b) three-stage transition from FE first to SCLC then back to FE at large D. For $k > k_c$, the conventional two-stage transition from FE to SCLC will always occur for all D, including the classical case of $k = 2$. Using various unconventional FE models with $k \neq 2$, we specifically demonstrate these peculiar transitions. Under a normalized model, our findings uncover the rich interplay between the source-limited FE and bulk-limited SCLC over a wide range of operating conditions.

DOI: 10.1103/PhysRevApplied.16.064025

I. INTRODUCTION

Field emission (FE) describes the process of electron emission from a cathode via tunneling at a sufficiently high electric field, which is known as the Fowler-Nordheim (FN) law [1–3]:

$$J = \mathcal{A}{E_s}^2 \exp\left(-\frac{\mathcal{B}}{E_s}\right), \tag{1}$$

where J is the current density, E_s is the surface electric field, $\mathcal{A}$ and $\mathcal{B}$ are material- and structure-dependent parameters. At high field where J reaches a sufficiently large quantity, the space-charge effects become relevant and the FN law transitions into the space-charge-limited current (SCLC) or the Child-Langmuir (CL) law [4,5]:

$$J = \frac{4\epsilon_0}{9}\sqrt{\frac{2e}{m_e}}\frac{V^{3/2}}{D^2}, \tag{2}$$

where e and m_e are the charge and the mass of free electron, respectively, ϵ_0 is the free-space permittivity, V is the voltage, and D is the gap spacing. For a nanogap, the quantum CL law is $J \propto V^{1/2}$ [6]. The transition from the FN law to the CL law has been studied for a large gap [7–9], microgap [10], and nanogap [11,12], which is useful for diodes [13,14].

The conventional two-stage transition from FE to SCLC is based on the classical FN law having a scaling of $\ln\left(J/{E_s}^k\right) \propto {E_s}^{-1}$ with $k = 2$. This understanding seems to be challenged by the emergence of various conditions not obeying the classical emission models [15–20]. Examples of the FE model with $k \neq 2$ include Schottky-Nordheim (SN) barrier modification ($k \approx 1.23$ when $\phi_B = 4.5$ eV) [17], graphene ($k = 1.53$) [18], two-dimensional (2D) semimetals ($k = 1$) [19], and three-dimensional (3D) topological semimetals ($k = 3$) [20]. Note the $k \neq 2$ behavior of FE can be caused by surface roughness ($k < 2$) [21,22]. For thermionic emission, the deviation of the normal temperature scaling law has also been reported recently [23,24].

In this paper, we aim to study the transition from FE to SCLC for arbitrary values of k over a wide range of applied voltage V and gap spacing D. The main findings are summarized in Fig. 1. Intriguingly, there is a critical value $k_c \equiv 3/2$ that, for $k \leq k_c$, the transition to SCLC is no longer possible for small D [Figs. 1(d) and 1(e)]. For large D at $k < k_c$, the transition becomes a three-stage process: FE to SCLC to FE as shown in Fig. 1(e). For $k > k_c$, we have a two-stage transition from FE to SCLC for all values of D [Figs. 1(a) to 1(c)]. The abnormal transition arises solely because of unconventional FE having $k < k_c$, which fails to supply sufficient space charge to sustain the required CL law. The critical $k_c \equiv 3/2$ can be qualitatively explained by the 3/2-power scaling governed by the CL law [25]. It is not due to other effects due to quantum [26], emission area [27,28], sharpness [29], short pulse [30–32], and finite particles [33,34]. Note that a normalized model

[*]yeesin_ang@sutd.edu.sg
[†]ricky_ang@sutd.edu.sg

has been formulated, hence the predicted results are universal as long as the FE is in a general form of Eq. (3). While the model is derived only for a planar gap, we expect the critical $k_c \equiv 3/2$ is applicable to cylindrical and spherical gap, as these geometries have been shown to have the same voltage scaling of the planar CL law with a numerical constant difference (Eq. 8 in Ref. [25]).

II. MODEL

We consider a generalized FE model of

$$J = \mathcal{A}_k {E_s}^k \exp\left(-\frac{\mathcal{B}}{E_s}\right), \tag{3}$$

where k is an arbitrary *scaling* of the surface electric field E_s in the pre-exponential term, $\mathcal{A}_k$ and $\mathcal{B}$ are constants due to materials and other properties. For simplicity, Eq. (3) can be transformed into a normalized form of

$$\bar{J} = \bar{E}^k \exp\left(-\frac{1}{\bar{E}}\right), \tag{4}$$

with $\bar{J} = J/J_0, \bar{E} = E_s/E_0$. $E_0 = \mathcal{B}$ and $J_0 = \mathcal{A}_k \mathcal{B}^k$ are the characteristic electric field scale and current density scale, respectively, governed by the generalized FN law.

Using the same approach [7] in linking Eq. (4) to the Poisson equation in the Llewellyn form to account for the space-charge effects, we obtain

$$\frac{\bar{J}\bar{T}^2}{2} + \bar{E}\bar{T} = \sqrt{2\bar{V}}, \tag{5}$$

$$\frac{\bar{J}\bar{T}^3}{6} + \frac{\bar{E}\bar{T}^2}{2} = \bar{D}. \tag{6}$$

Here the other normalized variables are gap spacing $\bar{D} = D/D_0$, transit time $\bar{T} = T/T_0$, and voltage $\bar{V} = V/V_0$. Their respective scales are $D_0 = eE_0{T_0}^2/m_e$ (length), $T_0 = \varepsilon_0 E_0/J_0$ (time), and $V_0 = E_0 \times D_0$ (voltage). Once an emission model (or material) is specified with known $\mathcal{A}_k$ and $\mathcal{B}$, all the normalized constants can be calculated. Solving Eq. (5), we obtain $\bar{T} = \left(\xi_k/\bar{E}^{k-1}\right)\exp\left(1/\bar{E}\right)$, and

$$\xi_k = -1 + \sqrt{1 + 2\left(2\bar{V}\right)^{1/2}\bar{E}^{k-2}\exp\left(-\frac{1}{\bar{E}}\right)}, \tag{7}$$

which allows Eq. (6) to be rewritten as

$${\xi_k}^3 + 3{\xi_k}^2 = 6\bar{D}\bar{E}^{2k-3}\exp\left(-\frac{2}{\bar{E}}\right). \tag{8}$$

For given k and $\bar{D}$, Eqs. (7) and (8) are solved numerically to obtain $\bar{V}$ as a function of $\bar{E}$, which can be further used to calculate $\bar{J}$ via Eq. (4), and finally the relationship between $\bar{J}$, $\bar{D}$, and $\bar{V}$ is determined consistently.

The factor $\bar{E}^{2k-3}$ in Eq. (8) suggests two contrasting behaviors for $\bar{E} \gg 1$. For $2k > 3$, we have $6\bar{D}\bar{E}^{2k-3}\exp\left(-2/\bar{E}\right) \to 6\bar{D}\bar{E}^{2k-3}$. For $2k < 3$, the limit is $6\bar{D}\bar{E}^{2k-3}\exp\left(-2/\bar{E}\right) \to 0$. Such a contrasting limit of Eq. (8) at $\bar{E} \gg 1$ indicates the existence of a *critical* value of k defined as $k_c \equiv 3/2$, which classifies k into three different regimes: (i) $k > k_c$ (supercritical), (ii) $k = k_c$ (critical), and (iii) $k < k_c$ (subcritical).

In the supercritical regime at $k > k_c \equiv 3/2$, the normalized FE model at low field $\bar{E} \ll 1$ is

$$\bar{J}_{\mathrm{FE}} = \left(\frac{\bar{V}}{\bar{D}}\right)^k \exp\left(-\frac{\bar{D}}{\bar{V}}\right). \tag{9}$$

At high field $\bar{E} \gg 1$, we recover the normalized CL law:

$$\bar{J}_{\mathrm{SCLC}} \times \bar{D}^2 = \frac{4\sqrt{2}}{9} \times \bar{V}^{3/2}. \tag{10}$$

Detailed derivation of Eqs. (9) and (10) and their asymptotic limits at various regimes are shown in Appendix A. By equating Eqs. (9) and (10), we obtain a relationship between $\bar{V}$ and $\bar{D}$, which is

$$\frac{4\sqrt{2}}{9}\frac{\bar{V}^{3/2-k}}{\bar{D}^{2-k}} = \exp\left(-\frac{\bar{D}}{\bar{V}}\right). \tag{11}$$

III. RESULTS AND DISCUSSION

Solutions of Eq. (11) are plotted in Fig. 1 for different k = 1, 3/2, 1.75, 2, and 3 to show the boundary separating the FE-dominated and SCLC regimes as a function of $\bar{V}$ and $\bar{D}$. For supercritical cases with $k > k_c \equiv 1.5$ [i.e., $k = 3$, 2 and 1.75 in Figs. 1(a)–1(c)], the two-stage FE-to-SCLC transition is evident at increasing $\bar{V}$ with all $\bar{D}$. Such a classic transition is, however, no longer warranted for $k \leq 3/2$. For critical ($k = k_c \equiv 3/2$) and subcritical ($k = 1 < k_c$) cases, we have only the FE regime (complete absence of SCLC even at infinitely large V) when $\bar{D}$ is smaller than a critical value $\bar{D}_c$ [marked by the red dashed lines in Figs. 1(d) and 1(e)]. This critical $\bar{D}_c$ is defined as the minimum solution of $\bar{D}$ from Eq. (11) as plotted in Fig. 1(f) for $0 \leq k \leq 3/2$. For $\bar{D} > \bar{D}_c$, the two-stage transition (FE-to-SCLC) is only present in the critical case ($k = 1.5$) in Fig. 1(d). This is in stark contrast to the subcritical case ($k = 1$) in Fig. 1(e) for which the SCLC occurs only in the intermediate $\bar{V}$ regime before the FE becomes dominant again at high $\bar{V}$, which is the three-stage transition (FE-to-SCLC-to-FE). The actual value of the critical gap, D_c is dependent on the normalized constants of the governing FN law, and can be calculated with $D_c = D_0 \times \bar{D}_c$.

Figure 2 shows the calculated $\bar{J} \times \bar{D}^2$ as a function of $\bar{V}$ for various k. The normalized gap distances are specifically chosen at $\bar{D} = 100$ and $\bar{D} = 0.01$ to show a comparison between large $\bar{D}$ ($> \bar{D}_c$) and small $\bar{D}$ ($< \bar{D}_c$) cases. For $k =$

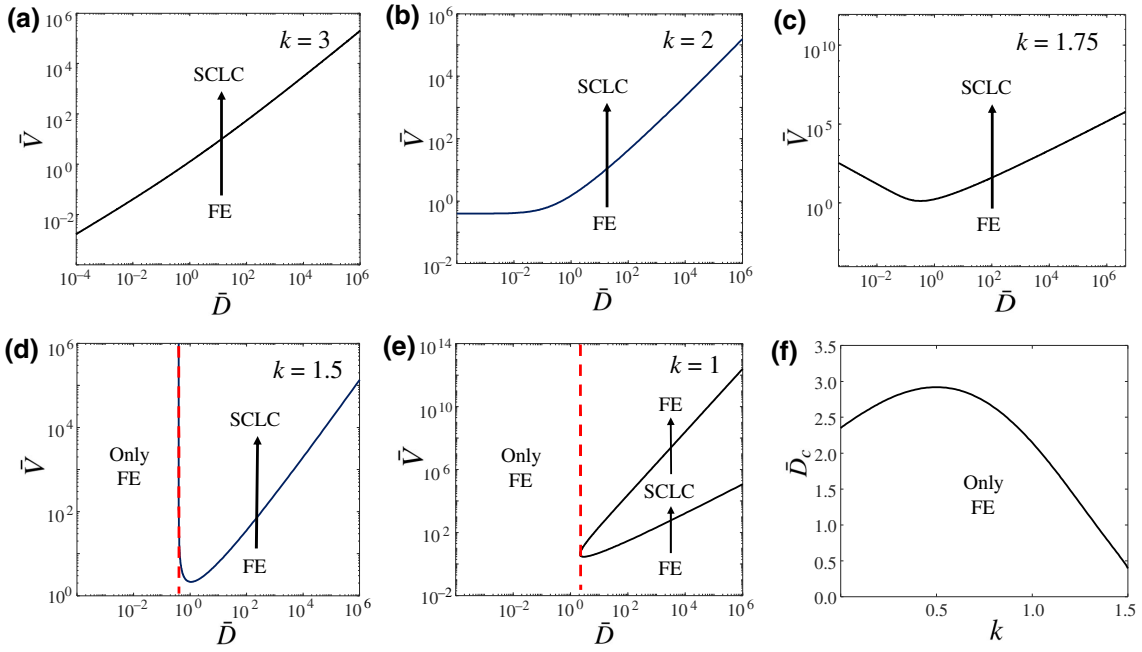

FIG. 1. Susceptibility diagram of FE and SCLC for normalized voltage $\bar{V}$ and normalized gap spacing $\bar{D}$. The solid line governs the transition between FE and SCLC for (a) $k = 3$, (b) $k = 2$, (c) $k = 1.75$, (d) $k = k_c \equiv 3/2$, and (e) $k = 1$. The red dashed lines in (d),(e) indicate the critical $\bar{D}_c$, which separates the exclusively only FE from the multiple-stage transition. (f) The critical $\bar{D}_c$ from $k = 0$ to $k_c \equiv 3/2$.

2 (supercritical cases), the results exhibit a smooth transition from FE to SCLC for both large and small $\bar{D}$ cases, which confirms the Fig. 1(b) scenario and thus also recovers the well-known classical transition [7]. As discussed above, this two-stage transition is no longer warranted for $k \leq 1.5$, and $\bar{D}$ will become a factor in determining the transition. For small $\bar{D} = 0.01$, Fig. 2(b) shows that transition from FE to SCLC is not possible for both $k = 1.5$ and $k = 1$, which confirm the results in Figs. 1(d) and 1(e). On the other hand, Fig. 2(a) confirms the three-stage transition at large $\bar{D} = 100$ for the $k = 1$ case, which is also depicted in Fig. 1(e). The three-stage transition arises because FE can only generate sufficient current density to maintain SCLC at moderate voltage, and thus back to FE at high voltage.

The above different transitions for various k and D are summarized in Fig. 1. The *exclusive and only* FE mechanism at $k \leq k_c \equiv 1.5$ and small $\bar{D} < \bar{D}_c$ arises due to not having sufficient emitted electrons to sustain the SCLC in a small gap spacing. Figure 2(b) also shows a significant reduced current density with decreasing k towards zero and saturation of J. If one can identify some FE models (or materials) with $k \approx 0$, this property may serve a favorable condition for stable current output even at high voltage [see Fig. 3(c) and 3(f)].

We now employ several examples at different k to illustrate the peculiar transition reported above for potential future experimental verification operating at high voltage. The details are discussed and their normalized constants are calculated in Appendix B. For fair comparison, let us

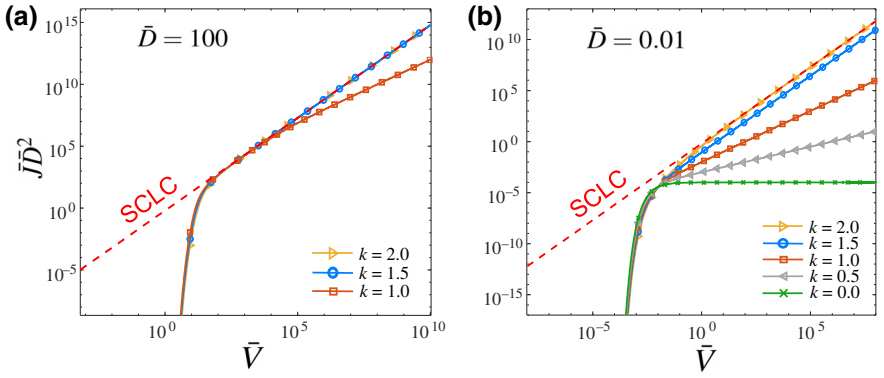

FIG. 2. Normalised $\bar{J}$-$\bar{V}$ characteristics of field emission with different k at (a) $\bar{D} = 100$, and (b) $\bar{D} = 0.01$. The red dashed lines represent the SCLC limit.

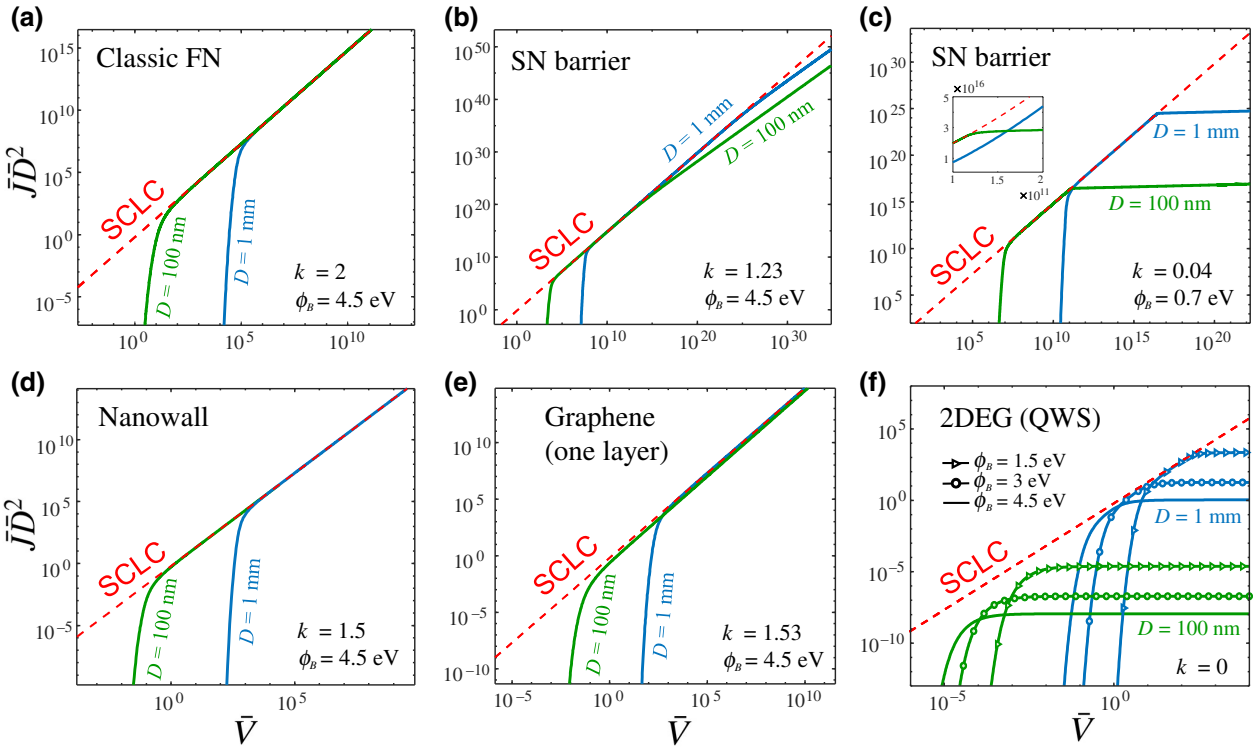

FIG. 3. $\bar{J}$-$\bar{V}$ curves of different field emission models at $D = 100$ nm and 1 mm. The work functions ϕ_B used for each model are labeled in the figures. The red dashed lines represent the SCLC limits.

consider work function $\phi_B = 4.5$ eV for five cases: classical FN law ($k = 2$), SN barrier ($k = 1.23$), nanowall ($k = 1.5$), monolayer graphene ($k = 1.53$), and 2DEG ($k = 0$) as shown in Figs. 3(a), 3(b), 3(d) 3(e), and 3(f), respectively. For each case, we use two gap spacings: $D = 1$ mm and 100 nm. For $D = 100$ nm, the FE-SCLC transition is at $\bar{V} = 26.47$ in Fig. 3(a), which corresponds to $V \approx 3 \times 10^3$ V or $E_s \approx 30$ V/nm. For $D = 1$ mm, we have $E_s \approx 10$ V/nm. This high field can be reduced by using a lower work function [see Figs. 3(c) and 3(f)].

The SN barrier model [17] has a more accurate barrier, and the k is calculated by $k = 2 - \eta/6$, where $\eta \equiv e^3 B_{\rm FN}/4\pi\epsilon_0\phi_B{}^{1/2}$ is a dimensionless work-function-dependent parameter. For $\phi_B = 4.5$ eV, we have $k \approx 1.23$ used in Fig. 3(b), which shows a lower transition voltage as compared to $k = 2$ in Fig. 3(a). Note Fig. 3(b) belongs to the subcritical case, where the emission eventually dwells back into the FE regime at high voltage due to the three-stage transition. However, the transition from SCLC back to FE will occur at an unrealistically high voltage, which is not feasible experimentally.

For the critical case at $k \approx k_c \equiv 1.5$, we consider nanowall ($k = 1.5$) and graphene ($k = 1.53$), which both converge to SCLC for both $D = 100$ nm and $D = 1$ mm. The graphene case is based on a Bardeen transfer Hamiltonian formalism [18]. The nanowall case is due to the quantum confinement effect leading to a quantized energy component along the confinement direction [35].

As mentioned before, transition from FE to SCLC at low field is feasible by using low work-function materials [36,37]. For $\phi_B = 0.7$ eV [36], the SN model gives $k = 0.04$, which shows a lower E-field of about 0.3 V/nm for both $D = 100$ nm and $D = 1$ mm [see Fig. 3(c)]. Here the $\bar{D}$ values are larger than the calculated $\bar{D}_c$ in Fig. 1(f), thus three-stage transition is possible at sufficiently high field. In Fig. 3(f), we show another $k = 0$ case by using the FE model of a 2DEG based on a (Al,Ga)As/GaAs quantum-well-structure (QWS) [38]. For this case, we have $D_c \approx 2.4 \times 10^{-3} = 2.4$ mm at $\phi_B = 4.5$ eV. In contrast to Fig. 3(c), we have the pure FE as expected in the subcritical regime due to small $D < D_c$. To illustrate the effect of work functions, the results at $\phi_B = 1.5$ to 4.5 eV are plotted in Fig. 3(f). The electron emission is exclusively FE at small $D = 100$ nm for all work functions. At $D = 1$ mm, the three-stage transition occurs only with small $\phi = 1.5$ eV.

IV. CONCLUSION

This paper shows that the conventional transition from the FE model at low voltage to SCLC at high voltage is no longer valid when FE does not follow the well-known FN

law. For unconventional FE emission with arbitrary k, our model predicts a critical value of $k_c \equiv 3/2$ for which some peculiar transitions will appear in three different regimes ($k > k_c$, $k = k_c$, and $k < k_c$) shown in Fig. 1. Recently, high-current-density field emission is demonstrated experimentally in 2D materials [39,40]. Such emitters, if operated at the high-field regime, can be used to verify our model. The reported findings provide a theoretical foundation for the modeling of unconventional field-emission materials as high-current electron sources useful for applications like high-power microwave sources, beam physics, and plasma physics. [41–44].

ACKNOWLEDGMENTS

We thank B. Lepetit for insightful discussions. This work is supported by Singapore MOE AcRF Tier 2 Grant (No. 2018-T2-1-007), A*STAR AME IRG Grant (No. A2083c0057) and SUTD Startup Grant (No. SRG SCI 2021 163).

APPENDIX A: ANALYTICAL FORMULATION OF THE ASYMPTOTIC BEHAVIORS

From the generalized current-density equation and the Llewellyn form of the Poisson equation [7], the normalized equations [which are Eqs. (4), (7), and (8)] can be derived as

$$\bar{J} = \bar{E}^k \exp\left(-\frac{1}{\bar{E}}\right), \tag{A1}$$

$$\xi_k = -1 + \sqrt{1 + 2\left(2\bar{V}\right)^{1/2} \bar{E}^{k-2} \exp\left(-\frac{1}{\bar{E}}\right)}, \tag{A2}$$

$$\xi_k{}^3 + 3\xi_k{}^2 = 6\bar{D}\bar{E}^{2k-3} \exp\left(-\frac{2}{\bar{E}}\right). \tag{A3}$$

These three equations can be solved numerically to obtain the relationship of $\bar{J}$, $\bar{V}$ or $\bar{E}$, $\bar{D}$ and k. We now analytically examine the asymptotic behaviors for (i) $k > k_c$; (ii) $k = k_c$; and (iii) $k < k_c$, where $k_c \equiv 3/2$.

1. Supercritical case: $k > k_c \equiv 3/2$

We first consider the most common case, $k > 3/2$, where the classic FN law fall in this supercritical regime with $k = 2$. At large $\bar{E} \gg 1$ limit, we have $\exp\left(-2/\bar{E}\right) \to 1$ and $\bar{E}^{2k-3} \gg 1$, the rhs of Eq. (A3) becomes $6\bar{D}\bar{E}^{2k-3} \gg 1$. Since $\xi_k \gg 1$, Eq. (A2) is dominated by the $\bar{E}$ term and it becomes

$$\xi_k \approx 2^{1/2} \left(2\bar{V}\right)^{1/4} \bar{E}^{(k-2)/2}. \tag{A4}$$

In doing so, $\xi_k \gg 1$ and the ξ_k-cubic term in Eq. (A3) dominates, which becomes

$$\xi_k{}^3 \approx 6\bar{D}\bar{E}^{2k-3}. \tag{A5}$$

Equating Eqs. (A4) and (A5), we obtain

$$2^{1/2} \left(2\bar{V}\right)^{1/4} \bar{E}^{k/2-1} = \left(6\bar{D}\bar{E}^{2k-3}\right)^{1/3}, \tag{A6}$$

which allows the surface electric field and the applied voltage to be related as

$$\bar{E} = \frac{2^{5/2k}}{3^{2/k}} \frac{\bar{V}^{3/2k}}{\bar{D}^{2/k}}. \tag{A7}$$

Inserting Eq. (A7) into Eq. (A1), we recover the classical CL law given by

$$\bar{J}_{k>1.5}\left(\bar{E} \to \infty\right) = \frac{4\sqrt{2}}{9} \frac{\bar{V}^{3/2}}{\bar{D}^2}. \tag{A8}$$

In the opposite limit of $\bar{E} \ll 1$, $\exp\left(-2/\bar{E}\right) \to 0$ and $\bar{E}^{2k-3} \to 0$. In this limit, $6\bar{D}\bar{E}^{2k-3} \exp\left(-2/\bar{E}\right) \ll 1$, $\xi_k \ll 1$. and the ξ_k-quadratic term in Eq. (A3) dominates, which yields

$$3\xi_k{}^2 \approx 6\bar{D}\bar{E}^{2k-3} \exp\left(-\frac{2}{\bar{E}}\right). \tag{A9}$$

Due to $\xi_k \ll 1$, the term containing $\bar{E}$ in the square-root term in Eq. (A2) is vanishingly small. By using Taylor expansion, we obtain

$$\xi_k \approx \left(2\bar{V}\right)^{1/2} \bar{E}^{k-2} \exp\left(-\frac{1}{\bar{E}}\right). \tag{A10}$$

Combining Eqs. (A9) and (A10), we get $3\left(2\bar{V}\right)\bar{E}^{2k-4} \exp\left(-2/\bar{E}\right) = 6\bar{D}\bar{E}^{2k-3} \exp\left(-2/\bar{E}\right)$, which can be simplified to yield $\bar{V} = \bar{D} \times \bar{E}$ that allows Eq. (A1) to recover the generalized FE current density:

$$\bar{J}_{k>1.5}\left(\bar{E} \to 0\right) = \left(\frac{\bar{V}}{\bar{D}}\right)^k \exp\left(-\frac{\bar{D}}{\bar{V}}\right). \tag{A11}$$

From the asymptotic limits of Eqs. (A11)and (A8), we prove the two-stage transition from FE at small field $\bar{E} \ll 1$ to the CL law (or SCLC) at large field $\bar{E} \gg 1$ for the $k > k_c$ case.

2. Critical case: $k = k_c \equiv 3/2$

In the critical regime at $k = k_c$, we show that other than the two-stage FE-to-SCLC transition, there exists another possible situation, where SCLC is absent in the emission

process for small $\bar{D} \ll 1$. At $k = 1.5$, we get $\bar{E}^{2k-3} = 1$, Eq. (A3) is

$$\xi_k{}^3 + 3\xi_k{}^2 = 6\bar{D}\exp\left(\frac{1}{\bar{E}}\right). \tag{A12}$$

Consider $\bar{D} \gg 1$, we have $\bar{D}\exp\left(1/\bar{E}\right) \gg 1$ and $\bar{D}\exp\left(1/\bar{E}\right) \ll 1$ for $\bar{E} \gg 1$ and $\bar{E} \ll 1$, respectively. This is similarly to the supercritical case, where a two-stage FE-to-SCLC transition is expected, given by

$$\bar{J}_{k=1.5}\left(\bar{D} \gg 1, \bar{E} \to \infty\right) = \frac{4\sqrt{2}}{9}\frac{\bar{V}^{3/2}}{\bar{D}^2}, \tag{A13}$$

$$\bar{J}_{k=1.5}\left(\bar{D} \gg 1, \bar{E} \to 0\right) = \left(\frac{\bar{V}}{\bar{D}}\right)^k \exp\left(-\frac{\bar{D}}{\bar{V}}\right). \tag{A14}$$

However, for $\bar{D} \ll 1$, with any values of $\bar{E}$, we have $\bar{D}\exp\left(1/\bar{E}\right) \ll 1$. In this case, $\xi_k \ll 1$, the dominating term in Eq. (A3) is the ξ_k-quadratic term, and thus Eq. (A3) becomes

$$3\xi_k{}^2 \approx 6\bar{D}\exp\left(-\frac{2}{\bar{E}}\right). \tag{A15}$$

The case is now analogous to the small $\bar{E}$ limit in the supercritical case [see Eq. (A10)], and the generalized current voltage FE current density is recovered:

$$\bar{J}_{k=1.5}\left(\bar{D} \ll 1\right) = \left(\frac{\bar{V}}{\bar{D}}\right)^k \exp\left(-\frac{\bar{D}}{\bar{V}}\right). \tag{A16}$$

Thus at the critical regime $k = 1.5$ and $\bar{D} \ll 1$, the emission is an exclusively field emission without any transition to SCLC.

3. Subcritical case: $k < k_c \equiv 3/2$

We now consider the case of $k < 3/2$. In this regime, a peculiar three-stage FE-to-SCLC-to-FE transition could exist. At large $\bar{E} \gg 1$, we have $\bar{E}^{2k-3} \ll 1$, $\exp\left(-2/\bar{E}\right) \approx 1$, and $\xi_k \ll 1$. The conditions are exactly the same to the supercritical case of $k > 1.5$ at small $\bar{E} \ll 1$. Following the same procedure, it is found that the limit at large $\bar{E} \gg 1$ follows the FE limit rather than the SCLC limit

$$J_{k<1.5}(\bar{E} \to \infty) = \left(\frac{\bar{V}}{\bar{D}}\right)^k \exp\left(-\frac{\bar{D}}{\bar{V}}\right). \tag{A17}$$

When $\bar{E}$ is decreasing from the large $\bar{E}$ limit to the small $\bar{E}$ limit, for large $\bar{D}$, there is an intermediate $\bar{E}$ region, which gives $6\bar{D}\bar{E}^{2k-3}\exp\left(-2/\bar{E}\right) \gg 1$. In this scenario, $\xi_k \gg 1$, the cubic ξ_k term dominates, and Eq. (A3) thus approaches

$$\xi_k{}^3 \approx 6\bar{D}\bar{E}^{2k-3}\exp\left(-\frac{2}{\bar{E}}\right). \tag{A18}$$

Since $\xi_k \gg 1$, we can rewrite Eq. (A2) as

$$\xi_k \approx 2^{1/2}\left(2\bar{V}\right)^{1/4}\bar{E}^{(k-2)/2}\exp\left(-\frac{1}{2\bar{E}}\right). \tag{A19}$$

By combining Eqs. (A18) and (A19), we get the following relation:

$$\bar{E} = \frac{2^{5/2k}}{3^{2/k}}\frac{\bar{V}^{3/2k}}{\bar{D}^{2/k}}\exp\frac{1}{k\bar{E}}, \tag{A20}$$

which is substituted to Eq. (A1) to yield the SCLC limit given by

$$\bar{J}_{k<1.5}\left(\bar{E}_{\text{int}}\right) = \frac{4\sqrt{2}}{9}\frac{\bar{V}^{3/2}}{\bar{D}^2}. \tag{A21}$$

Finally at $\bar{E} \to 0$, the FE limit is obtained:

$$\bar{J}_{k<1.5}\left(\bar{E} \to 0\right) = \left(\frac{\bar{V}}{\bar{D}}\right)^k \exp\left(-\frac{\bar{D}}{\bar{V}}\right). \tag{A22}$$

Thus, for $k < k_c \equiv 3/2$, there exists two different transitions: (i) an exclusively FE at $\bar{D} \ll 1$; and (ii) three-stage FE-to-SCLC-to-FE transition at $\bar{D} \gg 1$.

APPENDIX B: NORMALIZED PARAMETERS OF DIFFERENT FIELD-EMISSION MODELS

In this section, we show the various FE models with different prefactor field-scaling exponents k used in Fig. 3. The normalized constants of each model are stated clearly and are calculated in the tables below.

1. Classic Fowler-Nordheim model

The classic FN law [1] has the following form of

$$J_{\text{FN}} = A_{\text{FN}}\frac{{E_s}^2}{\phi_B}\exp\left(-\frac{B_{\text{FN}}{\phi_B}^{3/2}}{E_s}\right), \tag{B1}$$

where A_{FN} and B_{FN} are the first and second Fowler-Nordheim constants, respectively. The classic FN equation can be easily rearranged into our normalized form with $\mathcal{A}_k \equiv A_{\text{FN}}/\phi_B$, $\mathcal{B} \equiv B_{\text{FN}}{\phi_B}^{3/2}$, and $k = 2$.

2. Schottky-Nordheim model

A more complete FN-type equation taking into account the different barrier shape is known as the SN model [17]

given by

$$J = A_{\mathrm{FN}} \frac{{E_s}^2}{\phi_B} \exp\left(-\frac{\nu_F B_{\mathrm{FN}} {\phi_B}^{3/2}}{E_s}\right), \tag{B2}$$

where ν_F is the barrier correction factor written as

$$\nu_F \approx 1 - \left(\frac{E_s}{E_r}\right) + \frac{1}{6}\left(\frac{E_s}{E_r}\right) \ln\left(\frac{E_s}{E_r}\right), \tag{B3}$$

and $E_r = 4\pi\epsilon_0 {\phi_B}^2/e^3$. Substituting Eq. (B3) to Eq. (B2) gives the following approximate equation:

$$J_{\mathrm{SN}} = A_{\mathrm{FN}} (\exp\eta) \frac{{E_r}^{\eta/6} {E_s}^{2-\eta/6}}{\phi_B} \exp\left(-\frac{B_{\mathrm{FN}} {\phi_B}^{3/2}}{E_s}\right), \tag{B4}$$

where $\eta \equiv B_{\mathrm{FN}} e^3/4\pi\epsilon_0 {\phi_B}^{1/2}$ is a dimensionless work-function-dependent parameter. The normalized constants are $\mathcal{A}_k \equiv A_{\mathrm{FN}} (\exp\eta) {E_r}^{\eta/6}/\phi_B$, $\mathcal{B} \equiv B_{\mathrm{FN}} {\phi_B}^{3/2}$, and $k = 2 - \eta/6$. For a work function of 4.5 eV, we have $k = 1.23$.

3. Graphene

Based on the Bardeen transfer Hamiltonian formalism, the graphene FE model can be approximated by [18]

$$J_{\mathrm{gr}} = \frac{e^3 {E_c}^{0.47} {E_s}^{1.53}}{16\pi^2\hbar W} \exp\left[-\frac{4}{3}\left(\frac{2m}{\hbar^2}\right)^{1/2} \frac{W^{3/2}}{eE_s}\right], \tag{B5}$$

where $E_c = 1\ \mathrm{V\,m^{-1}}$ is a characteristic field scale, W is a fitting parameter and has a value of 12.78 eV. This equation gives $\mathcal{A}_k \equiv e^3 {E_c}^{0.47}/\left(16\pi^2\hbar W\right)$, $\mathcal{B} \equiv (4/3)\left(2m/\hbar^2\right)^{1/2} W^{3/2}/e$, and $k = 1.53$.

4. 2DEG

Using the Bardeen transfer Hamiltonian formalism, the FE model for 2DEG is found to be [18]

$$J_{\mathrm{2DEG}} = \frac{e(2m_e)^{1/2}}{\pi\hbar^2} W_B (\phi_B + W_B)^{1/2} |\varphi(z)|^2 \exp\left[-\frac{4}{3}\left(\frac{2m_e}{\hbar^2}\right)^{1/2} \frac{(\phi_B + W_B)^{3/2}}{eE_s}\right], \tag{B6}$$

where $W_B = \pi\hbar^2 n/m_e$ is the width of the valence band, n is the charge-carrier concentration and $|\varphi(z)|^2 \approx 1/L$ where L is the thickness of the 2DEG. Using the (Al,Ga)As/GaAs QWS as an example of 2DEG, the thickness and the charge-carrier concentration are $L = 2$ nm and $n = 2 \times 10^{12}\ \mathrm{cm^{-2}}$, respectively [38]. Rearranging the above equation into the generalized form gives $\mathcal{A}_k \equiv e(2m_e)^{1/2} W_B (\phi_B + W_B) |\varphi(z)|^2/\pi\hbar^2$, $\mathcal{B} \equiv (4/3)\left(2m_e/\hbar^2\right)^{1/2} (\phi_B + W_B)^{3/2}/e$, and $k = 0$.

5. Nanowall

In the electron FE from a nanowall structure, when the nanowall width w is small enough, the emission is dominated by $n = 1$ sub-band [35]. This condition yields the following nanowall FE model:

$$J_{\mathrm{NW}} = A_{\mathrm{NW}} {\Theta_1}^{3/2} \frac{{E_s}^{3/2}}{w{H_1}^{3/4}} \exp\left(\frac{-B_{\mathrm{FN}} {H_1}^{3/2}}{\Gamma_1 E_s}\right), \tag{B7}$$

where $A_{\mathrm{NW}} \approx 1.079\,631 \times 10^{-10}\ \mathrm{A\,m^{-1}\,eV^{3/4}\,V^{-3/2}\,m^{3/2}}$ is a universal constant, $H_1 \approx \phi_B + (\pi\hbar/w)^2/2m_e$ is the barrier zero-field height seen by the tunneling electron in the $n = 1$ sub-band. Θ_1 and Γ_1 are dimensionless correction factors and have the following relations:

$${\Theta_1}^{-1} = \frac{1}{2}\int_0^1 \sqrt{\frac{\left(\rho^2 + {\xi_1}^2 t^2\right)}{(1-t)\left(1 + {\xi_1}^2 t^2\right)}}\, dt, \tag{B8}$$

$${\Gamma_1}^{-1} = \frac{3}{2}\int_0^1 \sqrt{\frac{(1-t)\left(\rho^2 + {\xi_1}^2 t^2\right)}{\left(1 + {\xi_1}^2 t^2\right)}}\, dt, \tag{B9}$$

where $\rho \approx 2\pi^{-1/2} (w/2h)^{1/2}$, $\xi_1 \approx H_1/eE_s h$, and h is the height of the nanowall. For a nanowall's width $w = 2$ nm, $h = 20$ nm, and $\phi_B = 4.5$ eV, we get $H_1 \approx 4.594$ eV and $\rho = 0.2523$. Due to the existence of the complicated field-dependent correction factors, the nanowall FE model cannot be directly rearranged into our generalized form. Hence, Eq. (B7) is rearranged into a different generalized

TABLE I. Normalized parameters of different FE models. The work function is set to $\phi_B = 4.5$ eV, except for the SN barrier model in which a lower work function of 0.7 eV is used.

Field-emission model	k	$\mathcal{A}_k$ ($\mathrm{A\,V^{-k}m^{k-2}}$)	$\mathcal{B}$ ($\mathrm{V\,m^{-1}}$)
Classic FN law	2	3.4254×10^{-7}	6.5207×10^{10}
SN barrier ($\phi_B = 4.5$ eV)	1.2272	2.4603×10^{3}	6.5207×10^{10}
SN barrier ($\phi_B = 0.7$ eV)	0.0406	1.4660×10^{16}	4.0006×10^{9}
Nanowall ($w = 2$ nm)	1.5	0.0172	6.7261×10^{10}
Graphene	1.53	0.0021	3.1062×10^{11}
2DEG (QWS)	0	2.0141×10^{12}	6.5311×10^{10}

TABLE II. Normalized constants of different FE models. The work function is set to $\phi_B = 4.5$ eV, except for the SN barrier model in which a lower work function of 0.7 eV is used.

Field-emission model	E_0 (V m^{-1})	J_0 (A m^{-2})	D_0 (m)	U_0 (V)
Classic FN law	6.5207×10^{10}	1.4565×10^{15}	1.7973×10^{-9}	117.20
SN barrier ($\phi_B = 4.5$ eV)	6.5207×10^{10}	4.5950×10^{16}	1.8057×10^{-12}	0.1177
SN barrier ($\phi_B = 0.7$ eV)	4.0006×10^{9}	3.5973×10^{16}	6.8039×10^{-16}	2.7220×10^{-6}
Nanowall ($w = 2$ nm)	6.7261×10^{10}	3.0009×10^{14}	4.6466×10^{-8}	3.1254×10^{3}
Graphene	3.1062×10^{11}	8.0414×10^{14}	6.3734×10^{-7}	1.9797×10^{5}
2DEG (QWS)	6.5311×10^{10}	2.0141×10^{12}	9.4436×10^{-4}	6.1677×10^{7}

form:

$$J_{\mathrm{NW}} = \mathcal{A}_k {\Theta_1}^{3/2} {E_s}^{3/2} \exp\left(-\frac{\mathcal{B}}{\Gamma_1 E_s}\right), \tag{B10}$$

where $\mathcal{A}_k \equiv A_{\mathrm{NW}}/w{H_1}^{3/4}$, $\mathcal{B} \equiv B_{\mathrm{FN}}{H_1}^{3/2}$, and $k \approx 1.5$.

With $\mathcal{B} \equiv B_{\mathrm{FN}}H_1^{3/2}$, $\mathcal{A} \equiv A_{\mathrm{NW}}/wH_1^{3/4}$, and $k = 0$, the nanowall field-emission model can be normalized to become

$$\bar{J}_{\mathrm{NW}} = \Theta_1^{3/2} \bar{E}^{3/2} \exp\left(-\frac{1}{\Gamma_1 \bar{E}}\right). \tag{B11}$$

Finally, the normalized parameters of these FE models are summarized in Table I. Using these parameters, the corresponding normalized constants are calculated with $E_0 \equiv \mathcal{B}, J_0 \equiv \mathcal{A}_k \mathcal{B}^k, T_0 \equiv \epsilon_0 E_0/J_0, D_0 \equiv eE_0{T_0}^2/m_e$, $U_0 \equiv E_0 D_0$, and shown in Table II.

[1] R. H. Fowler and L. Nordheim, Electron emission in intense electric fields, Proc. R. Soc. London A119, 173 (1928).

[2] E. L. Murphy and R. H. Good, Thermionic emission, field emission, and the transition region, Phys. Rev. **102**, 1464 (1956).

[3] R. G. Forbes, Comments on the continuing widespread and unnecessary use of a defective emission equation in field emission related literature, J. Appl. Phys. **126**, 210901 (2019).

[4] C. D. Child, Discharge from hot CaO, Phys. Rev. (Series I) **32**, 492 (1911).

[5] I. Langmuir, The effect of space charge and residual gases on thermionic currents in high vacuum, Phys. Rev. **2**, 450 (1913).

[6] L. K. Ang, T. J. T. Kwan, and Y.-Y. Lau, New Scaling of Child-Langmuir law in the Quantum Regime, Phys. Rev. Lett. **91**, 208303 (2003).

[7] Y. Y. Lau, Y. Liu, and R. K. Parker, Electron emission: From the Fowler–Nordheim relation to the Child–Langmuir law, Phys. Plasmas **1**, 2082 (1994).

[8] Y. Feng and J. P. Verboncoeur, Transition from Fowler-Nordheim field emission to space charge limited current density, Phys. Plasmas **13**, 073105 (2006).

[9] A. Rokhlenko, K. L. Jensen, and J. L. Lebowitz, Space charge effects in field emission: One dimensional theory, J. Appl. Phys. **107**, 014904 (2010).

[10] K. Torfason, Á. Valfells, and A. Manolescu, Molecular dynamics simulations of field emission from a planar nanodiode, Phys. Plasmas **22**, 033109 (2015).

[11] W. S. Koh and L. K. Ang, Transition of field emission to space-charge-limited emission in a nanogap, Appl. Phys. Lett. **89**, 183107 (2006).

[12] W. S. Koh and L. K. Ang, Quantum model of space–charge-limited field emission in a nanogap, Nanotechnology **19**, 235402 (2008).

[13] P. Zhang, Á. Valfells, L. K. Ang, J. W. Luginsland, and Y. Y. Lau, 100 years of the physics of diodes, Appl. Phys. Lett. **4**, 011304 (2017).

[14] P. Zhang, Y. S. Ang, A. L. Garner, Á. Valfells, J. W. Luginsland, and L. K. Ang, Space–charge limited current in nanodiodes: Ballistic, collisional, and dynamical effects, J. Appl. Phys. **129**, 100902 (2021).

[15] Y. S. Ang, S. J. Liang, and L. K. Ang, Theoretical modeling of electron emission from graphene, MRS Bull. **42**, 505 (2017).

[16] Y. S. Ang, L. Cao, and L. K. Ang, Physics of electron emission and injection in two-dimensional materials: Theory and simulation, InfoMat **3**, 502 (2021).

[17] R. G. Forbes, Use of Millikan–Lauritsen plots, rather than Fowler–Nordheim plots, to analyze field emission current-voltage data, J. Appl. Phys. **105**, 114313 (2009).

[18] B. Lepetit, A quantum mechanical model of electron field emission from two dimensional materials. Application to graphene, J. Appl. Phys. **129**, 144302 (2021).

[19] Y. S. Ang, C. H. Lee, and L. K. Ang, arXiv:2003.14004.

[20] W. J. Chan, Y. S. Ang, and L. K. Ang, arXiv:2105.09874.

[21] M. Zubair, Y. S. Ang, and L. K. Ang, Fractional Fowler–Nordheim law for field emission from rough surface with nonparabolic energy dispersion, IEEE Trans. Electron Devices **65**, 2089 (2018).

[22] M. Zubair and L. K. Ang, Fractional-dimensional Child-Langmuir law for a rough cathode, Phys. Plasmas **23**, 072118 (2016).

[23] Y. S. Ang, H. Y. Yang, and L. K. Ang, Universal Scaling Laws in Schottky Heterostructures Based on Two-Dimensional Materials, Phys. Rev. Lett. **121**, 056802 (2018).

[24] S.-J. Liang and L. K. Ang, Electron Thermionic Emission from Graphene and a Thermionic Energy Converter, Phys. Rev. Appl. **3**, 014002 (2015).

[25] Y. B. Zhu, P. Zhang, Á. Valfells, L. K. Ang, and Y. Y. Lau, Novel Scaling Laws for the Langmuir-Blodgett Solutions in Cylindrical and Spherical Diodes, Phys. Rev. Lett. **110**, 265007 (2013).

[26] Y. Y. Lau, D. Chernin, D. G. Colombant, and P.-T. Ho, Quantum Extension of Child-Langmuir Law, Phys. Rev. Lett. **66**, 1446 (1991).
[27] J. W. Luginsland, Y. Y. Lau, and R. M. Gilgenbach, Two-Dimensional Child-Langmuir law, Phys. Rev. Lett. **77**, 4668 (1996).
[28] Y. Y. Lau, Simple Theory for the Two-Dimensional Child-Langmuir Law, Phys. Rev. Lett. **87**, 278301 (2001).
[29] Y. B. Zhu and L. K. Ang, Space charge limited current emission for a sharp tip, Phys. Plasmas **22**, 052106 (2015).
[30] Á. Valfells, D. W. Feldman, M. Virgo, P. G. O'Shea, and Y. Y. Lau, Effects of pulse-length and emitter area on virtual cathode formation in electron guns, Phys. Plasmas **9**, 2377 (2002).
[31] L. K. Ang and P. Zhang, Ultrashort-Pulse Child-Langmuir Law in the Quantum and Relativistic Regimes, Phys. Rev. Lett. **98**, 164802 (2007).
[32] L. Wu and L. K. Ang, Nonequilibrium model of ultrafast laser-induced electron photofield emission from a DC-biased metallic surface, Phys. Rev. B **78**, 224112 (2008).
[33] A. Pedersen, A. Manolescu, and Á. Valfells, Space-Charge Modulation in Vacuum Microdiodes at THz Frequencies, Phys. Rev. Lett. **104**, 175002 (2010).
[34] Y. B. Zhu and L. K. Ang, Child–Langmuir law in the Coulomb blockade regime, Appl. Phys. Lett. **98**, 051502 (2011).
[35] X.-Z. Qin, W.-L. Wang, N.-S. Xu, Z.-B. Li, and R. G. Forbes, Analytical treatment of cold field electron emission from a nanowall emitter, including quantum confinement effects, Proc. R. Soc. A **467**, 1029 (2010).
[36] P. Schindler, D. C. Riley, I. Bargatin, K. Sahasrabuddhe, J. W. Schwede, S. Sun, P. Pianetta, Z.-X. Shen, R. T. Howe, and N. A. Melosh, Surface photovoltage-induced ultralow work function material for thermionic energy converters, ACS Energy Lett. **4**, 2436 (2019).
[37] R. M. Jacobs, D. Morgan, and J. H. Booske, in *2015 IEEE International Vacuum Electronics Conference (IVEC)* (2015), p. 1.
[38] R. J. Trew, in *15th International Conference on Microwaves, Radar and Wireless Communications*, Vol. 1 (2004), p. 18.
[39] E. Gruber, R. A. Wilhelm, R. Pétuya, V. Smejkal, R. Kozubek, A. Hierzenberger, B. C. Bayer, I. Aldazabal, A. K. Kazansky, F. Libisch, A. V. Krasheninnikov, M. Schleberger, S. Facsko, A. G. Borisov, A. Arnau, and F. Aumayr, Ultrafast electronic response of graphene to a strong and localized electric field, Nat. Commun. **7**, 13948 (2016).
[40] S. Tang, Y. Zhang, P. Zhao, R. Zhan, J. Chen, and S. Deng, Realizing the large current field emission characteristics of single vertical few-layer graphene by constructing a lateral graphite heat dissipation interface, Nanoscale **13**, 5234 (2021).
[41] J. H. Booske, Plasma physics and related challenges of millimeter-wave-to-terahertz and high power microwave generation, Phys. Plasmas **15**, 055502 (2008).
[42] J. H. Booske, R. J. Dobbs, C. D. Joye, C. L. Kory, G. R. Neil, G.-S. Park, J. Park, and R. J. Temkin, Vacuum electronic high power terahertz sources, IEEE Trans. Terahertz Sci. Technol. **1**, 54 (2011).
[43] M. Fuks and E. Schamiloglu, Rapid Start of Oscillations in a Magnetron with a Transparent Cathode, Phys. Rev. Lett. **95**, 205101 (2005).
[44] S. Korbly, A. Kesar, J. Sirigiri, and R. Temkin, Observation of Frequency-Locked Coherent Terahertz Smith-Purcell Radiation, Phys. Rev. Lett. **94**, 054803 (2005).